

Supporting Information

Modulating anti-inflammatory and anticancer properties by designing a family of metal-complexes based on 5-nitropicolinic acid

Amalia García-García,^{*a} Marta Medina-O'donnell,^b Sara Rojas,^a Mariola Cano-Merenilla,^b Juan Morales,^c M. Mar Quesada-Moreno,^c Juan Sainz,^b Iñigo J. Vitorica-Yrezabal,^a Antonio Rodríguez-Diéguez,^a Amparo Navarro ^{*c} and Fernando J. Reyes-Zurita ^{*b}

Table of contents

S1.	Selected bond length and angles.....	S2
S2.	Infrared spectroscopy.....	S4
S3.	Photophysical properties.....	S5
S4.	Cytotoxicity in cancer cell lines.....	S9
S5.	Chemical stability in solution.....	S10
S6.	Cytotoxic mechanism	S11
S7.	Anti-inflammatory studies.....	S12
S8.	Elemental analysis	S13
S9.	Single-crystal X-ray crystallographic data.....	S14
S10.	Theoretical calculations.....	S15

S1. Selected bond length and angles

Table S1 Selected bond lengths (\AA) and angles ($^\circ$) of coordination spheres for **1-6**.

Comp.	Bond	Distance (\AA)	Atoms	Angle ($^\circ$)
1	Mn-N1A	2.273(5)	O1A-Mn-N1A	101.99(19)
	Mn-O1A	2.147(4)	O1A-Mn-O2A	92.92(18)
	Mn-O2A	2.168(5)	O1A-Mn-N1B	88.89(18)
	Mn-N1B	2.295(5)	O1A-Mn-O1B	88.91(18)
	Mn-O1B	2.167(5)	O2A-Mn-N1A	73.87(18)
	Mn-O2B	2.176(5)	O2A-Mn-N1B	105.77(19)
			O2A-Mn-O2B	83.99(18)
			O1B-Mn-N1A	89.37(19)
			O1B-Mn-N1B	90.99(18)
			O1B-Mn-O2B	99.57(18)
			O2B-Mn-N1A	95.52(18)
			O2B-Mn-N1B	73.70(18)
2	Cd-N1A	2.347(8)	O1A-Cd-N1A	71.7(3)
	Cd-O1A	2.287(7)	O1A-Cd-O2A	99.5(2)
	Cd-O2A	2.309(7)	O1A-Cd-N1B	96.0(3)
	Cd-N1B	2.323(8)	O1A-Cd-O1B	81.9(2)
	Cd-O1B	2.296(7)	O2A-Cd-N1A	88.0(3)
	Cd-O2B	2.252(7)	O2A-Cd-N1B	89.5(3)
			O2A-Cd-O2B	86.3(2)
			O1B-Cd-N1A	109.4(3)
			O1B-Cd-N1B	72.3(3)
			O1B-Cd-O2B	99.0(2)
			O2B-Cd-N1A	88.3(3)
			O2B-Cd-N1B	104.3(3)
3	Cu-N1	1.949(4)	O1-Cu-N1	84.05(15)
	Cu-O1	1.943(3)	O1-Cu-N1'	95.95(15)
	Cu-O4	2.708(4)	O1-Cu-O4	94.90(13)
			O1-Cu-O4'	85.10(13)
			N1-Cu-O4	87.97(14)
			N1-Cu-O4'	92.03(14)
4	Co-N1	2.147(5)	O1-Co-N1	79.09(16)
	Co-O1	2.062(4)	O1-Co-N1'	100.91(16)
	Co-O1W	2.075(4)	O1-Co-O1W	89.32(14)
			O1-Co-O1W'	90.68(14)
			O1W-Co-N1	87.07(16)
			O1W-Co-N1'	92.93(16)
5	Ni-N1	2.084(4)	O1-Ni-N1	80.67(14)
	Ni-O1	2.049(3)	O1-Ni-N1'	99.33(14)
	Ni-O1W	2.054(3)	O1-Ni-O1W	90.97(13)
			O1-Ni-O1W'	89.03(13)
			O1W-Ni-N1	93.01(14)
			O1W-Ni-N1'	86.99(14)
6	Zn-N1	2.152(3)	O1-Zn-N1	79.36(9)
	Zn-O1	2.065(2)	O1-Zn-N1'	100.64(9)
	Zn-O1W	2.115(2)	O1-Zn-O1W	89.35(9)
			O1-Zn-O1W'	90.65(9)
			O1W-Zn-N1	87.21(10)
			O1W-Zn-N1'	92.79(10)

Table S2 Hydrogen bonds distances (\AA) and angles ($^\circ$) for **4-6**.

Comp.	D-H…A ^a	D-H distance	H…A distance	D-H…A distance	Angle ($^\circ$)
4	O1W-H1WA…O1	0.90	1.80	2.681(5)	164.2

	O1W-H1WB···O2	0.84	1.87	2.655 (5)	153.2
5	O1W-H1WA···O1	0.91	1.82	2.700 (5)	161.7
	O1W-H1WB···O2	0.85	1.86	2.665(5)	156.5
6	O1W-H1WA···O1	0.94	1.82	2.706(3)	156.3
	O1W-H1WB···O2	0.91	1.80	2.674(3)	160.3

^(a)D, donor atom; H, hydrogen atom; A, acceptor atom.

S2. Infrared spectroscopy

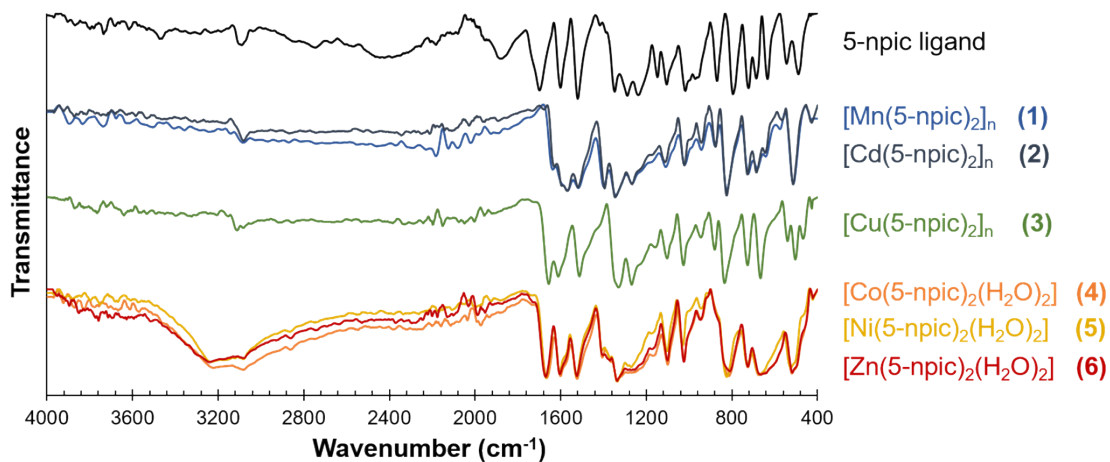


Fig. S1 Infrared spectra of 5-npic and compounds **1-6** in solid state in the range 4000-400 cm⁻¹ at room temperature.

Table S3 IR bands (cm⁻¹) in the range 4000-400 cm⁻¹ of 5-npic and compounds **1-6**.

	5-npic	1	2	3	4	5	6
$\delta(\text{O-H})$					3219	3232	3238
$\nu(\text{C-H})_{\text{aromatic}}$	3090 3078	3082 3082	3080 3082	3111 3111	3082	3082	3082
$\nu(\text{C=O})$	1728 1699	1635 1587	1629 1595	1655 1655	1664 1664	1668 1668	1670 1670
$\nu(\text{C=C})$	1601	1568	1568	1610	1601	1604	1604
$\nu_{\text{asym}}(\text{N-O})$	1520	1518	1518	1512	1523	1525	1525
$\nu_{\text{sym}}(\text{N-O})$	1348	1398	1394	1329	1334	1335	1336
$\nu(\text{C-N})$	1288	1342	1346	1267	1267	1269	1267
$\delta(\text{C-H})_{\text{in-plane}}$	1236 1018	1261 1020	1267 1022	1226 1026	1222 1022	1234 1030	1230 1024
$\delta(\text{C-C-C})_{\text{ring}}$	792	823	823	833	815	823	810

S3. Photophysical properties

Fig. S2 UV-vis absorption spectra in water (left) and emission spectra (right) of the ligand (black), compound **2** (red) and compound **6** (blue). Stokes shift estimated using the average value of the two bands at 283 and 248 nm of the absorption spectra and the main band at 485 nm of the emission spectra.

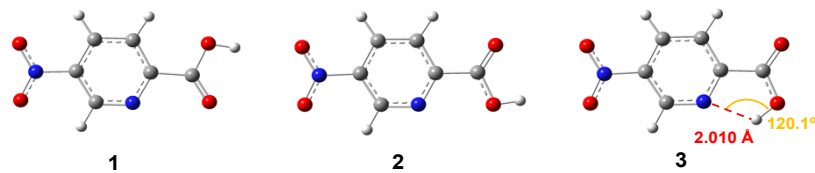


Fig. S3 Optimized conformations of 5-npic acid at the CAM-B3LYP/6-31G** level of theory in water solution.

Table S4 Energy (in Hartrees) of the three 5-nitropicolinic acid conformers, energy difference (ΔE , kcal/mol) with respect to the most stable conformer and dipole moment (μ , in Debye) calculated at the CAM-B3LYP/6-31G** level of theory in the gas phase and water solution.

Phase	Conformer	Energy	ΔE	μ
Gas	1	-641.089791	4.03	4.10
	2	-641.092370	2.42	2.47
	3	-641.096220	0.00	1.15
Water	1	-641.103986	3.07	5.31
	2	-641.104914	2.48	2.88
	3	-641.108871	0.00	1.55

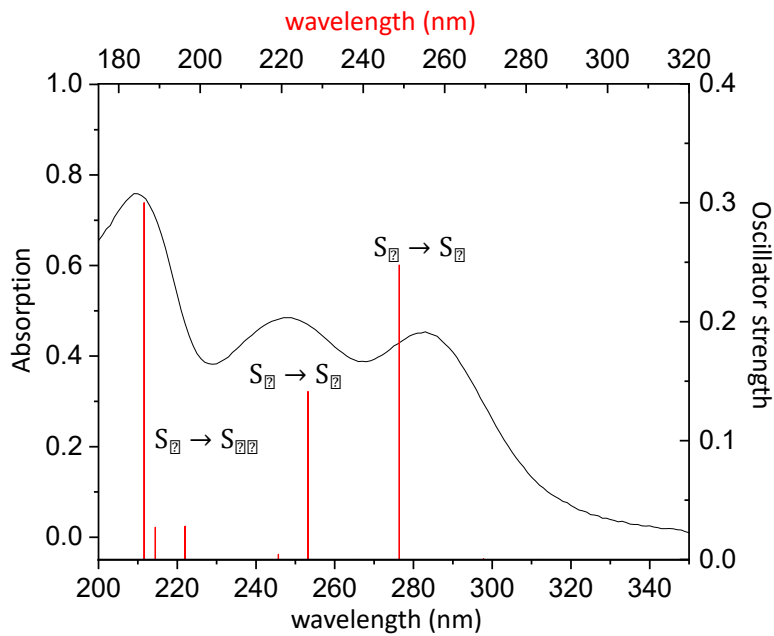


Fig. S4 Experimental absorption spectrum of 5-npic along with the oscillator strength of the vertical electronic transitions calculated at the TD-CAM-B3LYP/6-31G** level of theory in water solution. The bottom axis refers to the experimental absorption spectrum and the top axis to the calculated electronic transitions.

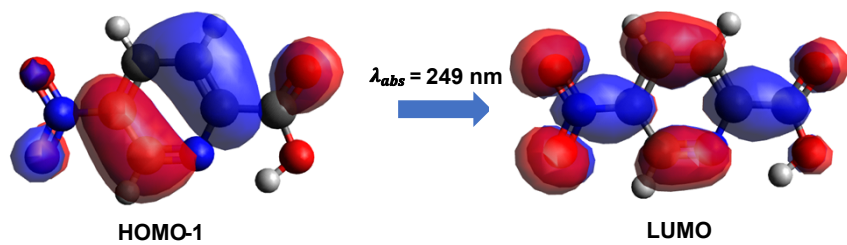


Fig. S5 Molecular orbital representation (isocontour plots 0.02 a.u.) of the electronic transition $S_0 \rightarrow S_4$ calculated at the CAM-B3LYP/6-31G** level of theory in water solution for the **conformer 3** of the ligand.

Table S5 Experimental absorption wavelength (λ_{ab}^{exp}), theoretical vertical electronic transitions ($\lambda_{vert-ab}^{calc}$), oscillator strength (f), and the main molecular orbital contributions ($\geq 15\%$) calculated at the CAM-B3LYP/6-31G** level of theory in water solution for the **conformer 3** of the ligand.

λ_{ab}^{exp} eV (nm)	$\lambda_{vert-ab}^{calc}$ eV (nm)	Transition	f	Contribution (%)
	4.01 (309)	$S_0 \rightarrow S_1$	0.00	HOMO-3 \rightarrow LUMO (80%)
4.38 (283)	4.98 (249)	$S_0 \rightarrow S_4$	0.25	HOMO-1 \rightarrow LUMO (88%)
5.00 (248)	5.48 (226)	$S_0 \rightarrow S_6$	0.14	HOMO-4 \rightarrow LUMO (69%)
	6.32 (196)	$S_0 \rightarrow S_8$	0.03	HOMO-5 \rightarrow LUMO (33%)
5.93 (209)	6.66 (186)	$S_0 \rightarrow S_{10}$	0.30	HOMO-6 \rightarrow LUMO (50%)

Table S6 Experimental emission (λ_{emis}^{exp}), theoretical transition ($\lambda_{vert-emis}^{calc}$), and oscillator strength (f) for the $S_1 \rightarrow S_0$ ($\geq 15\%$) calculated at the CAM-B3LYP/6-31G** level of theory in the gas phase and water solution for the **conformer 3** of the ligand.

Phase	λ_{emis} eV (nm)	$\lambda_{vert-emis}$ eV (nm)	Transition	f	Contribution (%)
Gas	2.56 (485)	2.03 (610)	$S_1 \rightarrow S_0$	0.00	LUMO \rightarrow HOMO (86%)
Water	2.56 (485)	2.37 (523)	$S_1 \rightarrow S_0$	0.00	LUMO \rightarrow HOMO (92%)

Table S7 Experimental absorption wavelength (λ_{ab}^{exp}), theoretical vertical electronic transitions ($\lambda_{vert-ab}^{calc}$), oscillator strength (f), and the main molecular orbital contributions ($\geq 15\%$) calculated at the CAM-B3LYP-D3/6-31G**+LANL2DZ level of theory in water solution for **6** (LANL2DZ for Zn, 6-31G** for C, H, N, and O).

λ_{ab} eV (nm)	$\lambda_{vert-ab}$ eV (nm)	ΔE (eV)	Transition	f	Contribution (%)
4.38 (283)	4.58 (271)	0.17	$S_0 \rightarrow S_7$	0.28	HOMO-8 \rightarrow LUMO (43%) HOMO-4 \rightarrow LUMO (41%)
4.98 (249)	4.93 (251)	-0.05	$S_0 \rightarrow S_{11}$	0.27	HOMO-6 \rightarrow LUMO+1 (52%) HOMO-3 \rightarrow LUMO+1 (27%)
5.79 (214)	7.52 (165)	1.73	$S_0 \rightarrow S_{66}$	0.93	HOMO-6 \rightarrow LUMO+5 (20%)

Table S8 Experimental absorption wavelength (λ_{ab}^{exp}), theoretical vertical electronic transitions ($\lambda_{vert-ab}^{calc}$), oscillator strength (f), and the main molecular orbital contributions ($\geq 15\%$) calculated at the ONIOM(CAM-B3LYP-D3:PM6) level of theory in the gas phase for **6** (LANL2DZ for Zn, 6-31G** for C, H, N, and O).

λ_{abs}^{exp} eV (nm)	$\lambda_{vert-ab}^{calc}$ eV (nm)	Transition	f	% Contribution
4.38 (283)	4.58 (271)	$S_0 \rightarrow S_9$	0.10	HOMO-3 \rightarrow LUMO+1 (29%), HOMO-2 \rightarrow LUMO (38%)
4.98 (249)	5.13(242)	$S_0 \rightarrow S_{15}$	0.38	HOMO-7 \rightarrow LUMO+1 (27%), HOMO-6 \rightarrow LUMO (36%)
	5.69(218)	$S_0 \rightarrow S_{24}$	0.17	HOMO-2 \rightarrow LUMO+2 (20%)
				HOMO-15 \rightarrow LUMO+1 (20%), HOMO-14 \rightarrow LUMO (22%), HOMO-7 \rightarrow LUMO+3 (18%), HOMO-6 \rightarrow LUMO+2 (20%)
5.79 (214)	6.66 (186)	$S_0 \rightarrow S_{43}$	0.40	

Table S9 Experimental absorption wavelength (λ_{ab}^{exp}), theoretical vertical electronic transitions ($\lambda_{vert-ab}^{calc}$), oscillator strength (f), and the main molecular orbital contributions ($\geq 15\%$) calculated at the CAM-B3LYP-D3/6-31G** level of theory for **2** (LANL2DZ for Cd, 6-31G** for C, H, N, and O).

Fragment	λ_{abs} eV (nm)	$\lambda_{vert-ab}$ eV (nm)	Transition	f	% Contribution
f1Cd		4.67 (266)	$S_0 \rightarrow S_{45}$	0.05	HOMO-8 \rightarrow LUMO+1 (18%)
	4.38(283)	4.84 (256)	$S_0 \rightarrow S_{57}$	0.16	HOMO-11 \rightarrow LUMO+3 (23%), HOMO-9 \rightarrow LUMO+3 (25%)
	4.98 (249)	4.88 (254)	$S_0 \rightarrow S_{60}$	0.22	HOMO-18 \rightarrow LUMO (24%)
	5.79(214)	5.26 (236)	$S_0 \rightarrow S_{76}$	0.11	HOMO-22 \rightarrow LUMO+1 (27%) HOMO-21 \rightarrow LUMO+1 (24%)
f4Cd		4.32 (287)	$S_0 \rightarrow S_{52}$	0.01	< 15%
		4.61 (269)	$S_0 \rightarrow S_{87}$	0.02	HOMO-8 \rightarrow LUMO+10 (53%)
		4.67 (266)	$S_0 \rightarrow S_{95}$	0.04	< 15%
	4.38(283)	4.84 (256)	$S_0 \rightarrow S_{132}$	0.17	< 15%
	4.98 (249)	4.92 (252)	$S_0 \rightarrow S_{147}$	0.12	< 15%
	5.79(214)	5.32(233)	$S_0 \rightarrow S_{238}$	0.09	HOMO-51 \rightarrow LUMO+4 (29%)

S4. Cytotoxicity in cancer cell lines

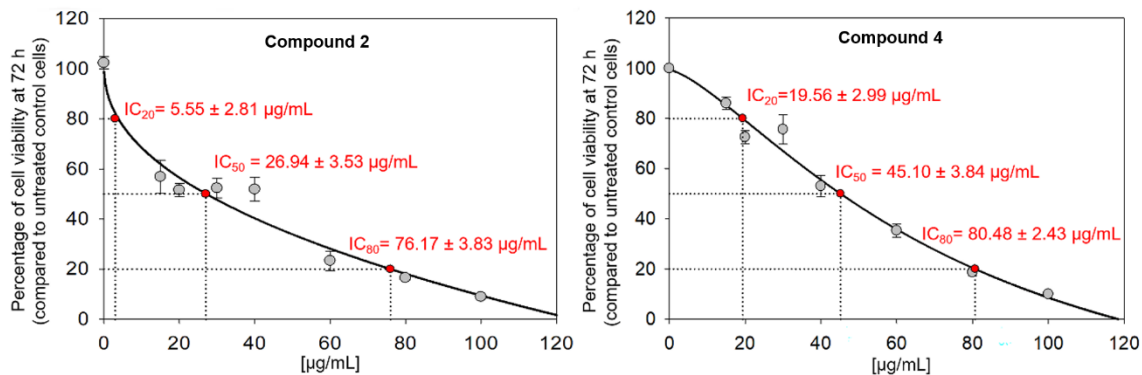


Fig. S6 Effect of **2** and **4** on cell proliferation in B16-F10 murine melanoma cells after 72 h of treatment in a range of concentration from 0 to 100 $\mu\text{g}\cdot\text{mL}^{-1}$. Each point represents the mean value \pm SD of at least two independent experiments performed in triplicate.

S5. Chemical stability in solution

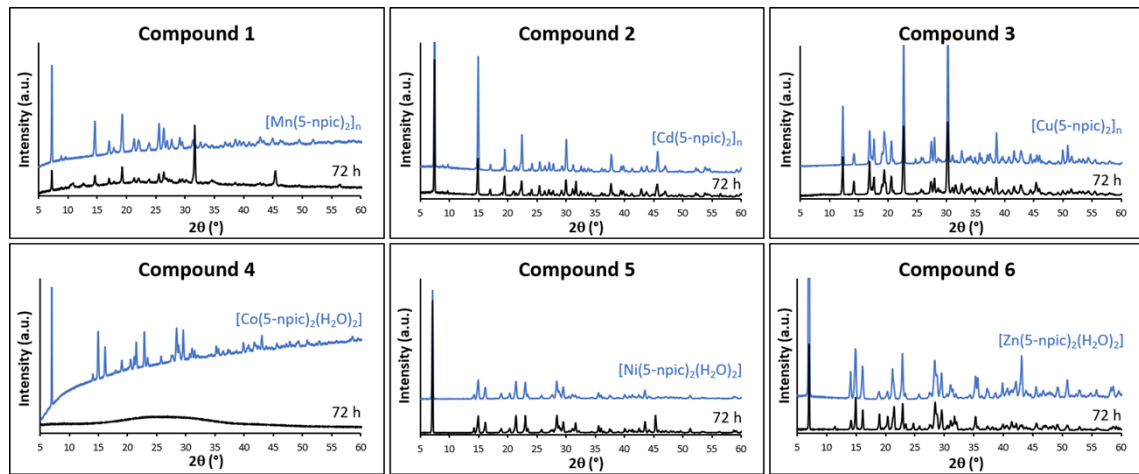


Fig S7. Powder X-ray diffraction patterns of complexes **1-6** after 72 h in PBS solution (black lines) compared to the original ones (blue lines). The patterns are registered from 5° to 60° with a step size of 0.02° and scan rate of 40 s per step.

S6. Cytotoxic mechanism

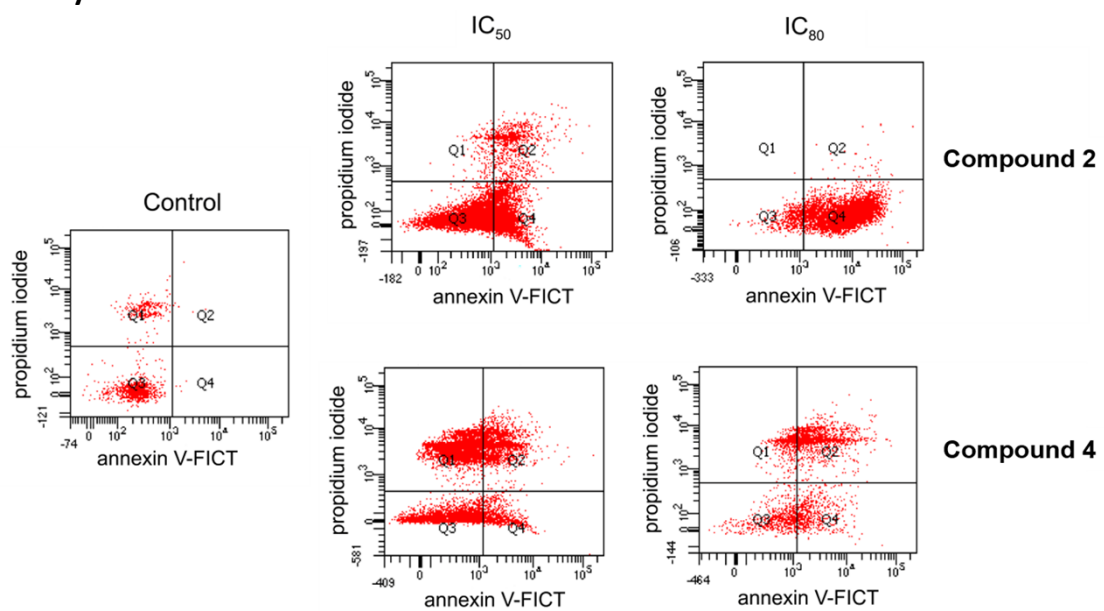


Fig. S8 Diagrams of annexin V/PI flow cytometry: Q1 (necrotic cells), Q2 (late apoptotic cells), Q3 (Viable cells), Q4 (early apoptotic cells).

S7. Anti-inflammatory studies

Table S10 Growth-inhibitory effects of ligand and compounds **1-6** on RAW 264.7 monocyte/macrophage murine cells.

Compound	IC ₂₀ ($\mu\text{g}\cdot\text{mL}^{-1}$)	IC ₅₀ ($\mu\text{g}\cdot\text{mL}^{-1}$)	IC ₈₀ ($\mu\text{g}\cdot\text{mL}^{-1}$)
L	47.43 ± 2.41	55.85 ± 0.88	66.46 ± 0.63
1	86.99 ± 5.89	134.38 ± 19.10	165.91 ± 11.46
2	1.96 ± 0.11	21.68 ± 0.06	74.86 ± 0.51
3	67.67 ± 4.15	86.90 ± 0.12	105.16 ± 4.96
4	39.85 ± 11.19	56.48 ± 3.69	71.88 ± 2.32
5	47.67 ± 2.33	59.32 ± 2.54	74.32 ± 3.40
6	29.05 ± 1.06	33.25 ± 0.57	38.76 ± 0.29

S8. Elemental analysis

Table S11 Elemental analyses (weight, %) of all obtained compounds.

Compound	Formula	Yield ^a (%)	Theoretical / Experimental (%)		
			C	H	N
1	C ₁₂ H ₆ MnN ₄ O ₈	97	37.04 / 36.96	1.55 / 1.79	14.40 / 14.68
2	C ₁₂ H ₆ CdN ₄ O ₈	92	32.27 / 32.24	1.35 / 1.56	12.54 / 12.63
3	C ₁₂ H ₆ CuN ₄ O ₈	75	36.23 / 35.72	1.52 / 1.70	14.09 / 14.32
4	C ₁₂ H ₁₀ CoN ₄ O ₁₀	93	33.58 / 33.62	2.35 / 2.64	13.05 / 13.37
5	C ₁₂ H ₁₀ NiN ₄ O ₁₀	80	33.60 / 33.51	2.35 / 2.72	13.06 / 13.20
6	C ₁₂ H ₁₀ ZnN ₄ O ₁₀	77	33.08 / 32.79	2.31 / 2.56	12.86 / 12.95

^a Yield based on metal

S9. Single-crystal X-ray crystallographic data

Table S12 Crystallographic data and structure refinement details.

	1	2	3	4	5	6
Formula	C ₁₂ H ₆ MnN ₄ O ₈	C ₁₂ H ₆ CdN ₄ O ₈	C ₁₂ H ₆ CuN ₄ O ₈	C ₁₂ H ₁₀ CoN ₄ O ₁₀	C ₁₂ H ₁₀ NiN ₄ O ₁₀	C ₁₂ H ₁₀ ZnN ₄ O ₁₀
CCDC	2295415	2295418	2295419	2295416	2295417	2295420
M_r (g·mol⁻¹)	389.15	446.61	397.75	429.17	428.95	435.61
T (K)	296.15	296.15	296.15	100.00	100.00	293(2)
Crystal system	Monoclinic	Monoclinic	Monoclinic	Monoclinic	Monoclinic	Monoclinic
Space group	P2 ₁	P2 ₁	P2 ₁ /c	P2 ₁ /n	P2 ₁ /n	P2 ₁ /n
a (Å)	10.4325(17)	10.5242(0)	6.4800(8)	5.0247(5)	5.0700(7)	5.0950(3)
b (Å)	5.3198(7)	5.4425(4)	10.0354(12)	25.069(3)	24.784(4)	25.1353(16)
c (Å)	12.7174(15)	12.4602(13)	10.6890(11)	6.4693(7)	6.4982(13)	6.5334(4)
α (°)	90	90	90	90	90	90
β (°)	108.111(4)	107.135(3)	106.370(4)	111.501(4)	111.764(6)	110.793(3)
γ (°)	90	90	90	90	90	90
V (Å³)	670.83(16)	662.02(11)	666.92(13)	758.20(15)	758.3(2)	782.20(8)
Z	2	2	2	2	2	2
ρ (g·cm⁻³)	1.927	2.175	1.981	1.880	1.879	1.850
μ (mm⁻¹)	1.044	1.660	1.697	1.202	1.350	1.638
GoF on F²	1.014	0.997	1.045	1.260	1.169	1.047
R₁^a [I>2σ(I)]	0.0543	0.0387	0.0280	0.0566	0.0654	0.0570
R₁^a [all data]	0.0799	0.0475	0.0323	0.1128	0.1532	0.1027
wR₂^b [I>2σ(I)]	0.0992	0.0725	0.0784	0.1366	0.1547	0.0846
wR₂^b [all data]	0.1125	0.0771	0.0805	0.1934	0.2380	0.0955

$$^a R_1 = \sum \frac{||F_o - |F_c||}{\sum |F_o|}, ^b wR_2 = \left[\sum w(|F_o^2| - |F_c^2|)^2 / \sum w(|F_o^2|) \right]^{1/2}$$

S10. Theoretical calculations

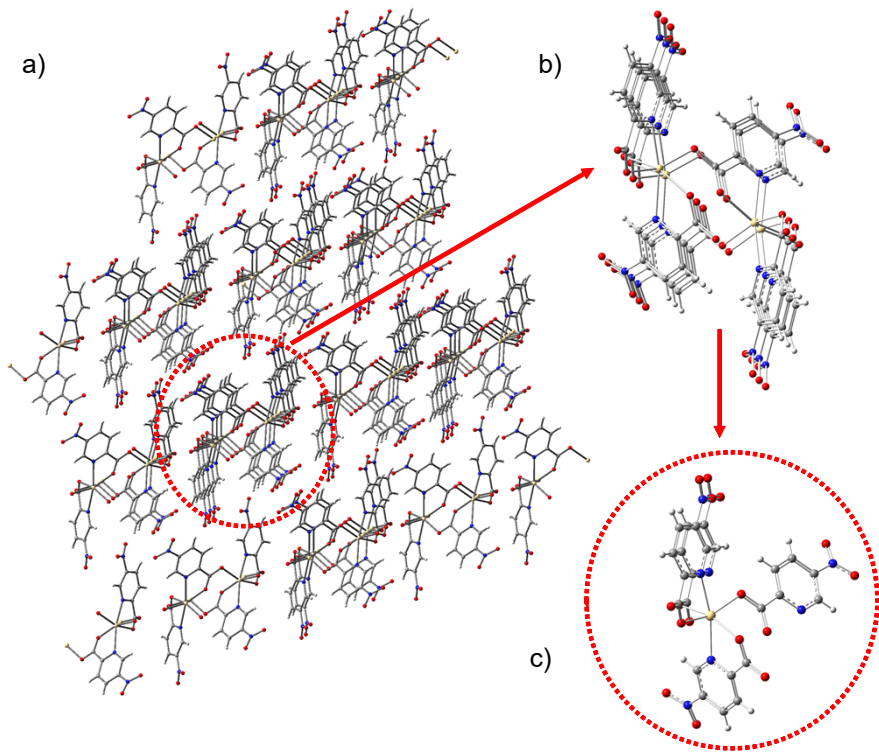


Fig. S9 Molecular representation of **2**: (a) schematic representation of the coordination compound; (b) **f4Cd** fragment containing four Cd atoms, and (c) **f1Cd** fragment containing one Cd atom.

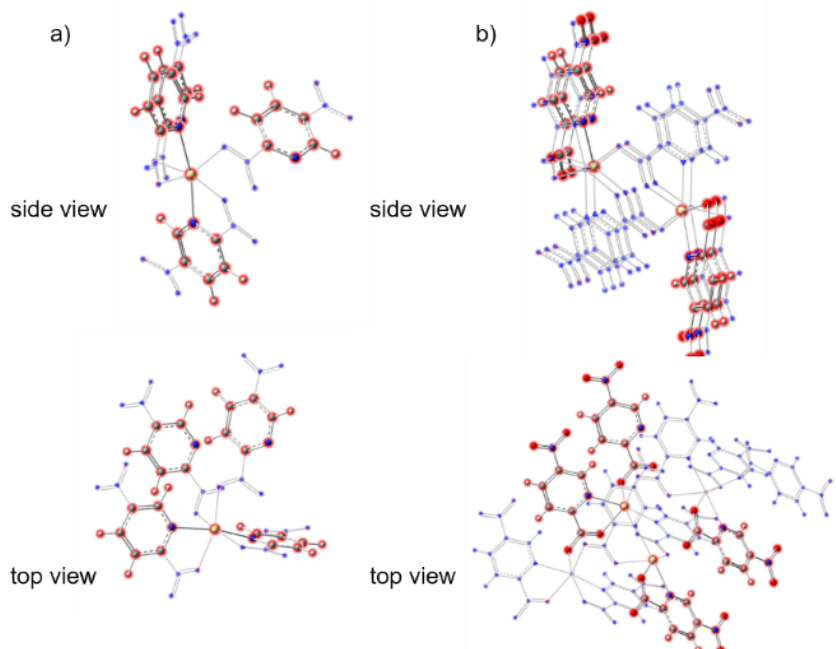


Fig. S10 (a) **f1Cd** fragment and (b) **f4Cd** fragment for **2**. The molecular geometry of the active part of the fragment (in red) has been optimized at the CAM-B3LYP-D3/6-31G**+LANL2DZ level of theory while the cartesian coordinates of the surrounding molecules (in blue) are frozen.

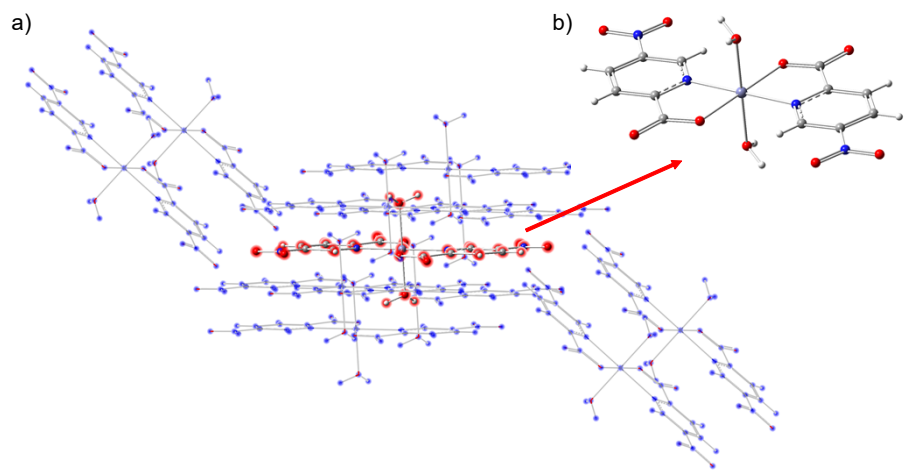


Fig. S11 (a) ONIOM model cluster of compound **6**. (b) The active molecule (in red) is treated as high level (CAM-B3LYP-D3/6-31G**+LANL2DZ) and the surrounding molecules (in blue) as low level (PM6).